Astron. Astrophys. 334, 201–209 (1998)

ASTRONOMY AND ASTROPHYSICS

Analyzing short-term X-ray variability of Cygnus X-1 with Linear State Space Models

Katja Pottschmidt, Michael König, Jörn Wilms, and Rüdiger Staubert

Institut für Astronomie und Astrophysik, Astronomie, University of Tübingen, Waldhäuser Strasse 64, D-72076 Tübingen, Germany

Received 7 October 1997 / Accepted 13 February 1998

Abstract. Cyg X-1 exhibits irregular X-ray variability on all measured timescales. The usually applied shot noise models describe the typical short-term behavior of this source by superposition of randomly occuring shots with a distribution of shot durations. We have reanalyzed EXOSAT ME observations of Cyg X-1 using the more general Linear State Space Models (LSSMs). These models, which explicitly take the observation-noise into account, model the intrinsic system variability with an autoregressive (AR) process. Our fits show that an AR process of first order can reproduce the system variability of Cyg X-1. A possible interpretation is again the superposition of individual shots, but with a single relaxation time τ. This parameter was found to be 0.19 s.

Key words: X-rays: stars – binaries: close – accretion, accretion disks – stars: individual: Cyg X-1 – methods: statistical

1. Introduction

The X-ray source Cyg X-1 was discovered by a rocket flight in 1964 (Bowyer et al. 1965). In March 1971 the sudden appearance of an accurately locateable radio source coinciding with a change in the luminosity of the X-ray source led to its identification with the O9.7 Iab supergiant HDE 226868 (Hjellming & Wade 1971; Bolton 1972). This star is known as part of a single lined spectroscopic binary system with an orbital period of 5.6 days at a distance of about 2.5 kpc. The X-ray emission of Cyg X-1 is produced by the accretion of material from the supergiant primary onto the compact object. According to Herrero et al. (1995), the most probable masses of the binary partners are $18\,M_\odot$ for the primary and $10\,M_\odot$ for the compact object, which is one of the most firmly established black hole candidates (BHCs). The accretion process is believed to be fueled by a focused stellar wind from HDE 226868 (Friend & Castor 1982).

During most of the time Cyg X-1 is emitting a non-thermal or hard state spectrum (for the soft state, cf. Cui et al. 1997), which can be described by a power-law with a photon-index $\Gamma \approx$1.5-1.7, modified by an exponential cutoff with a folding energy of about 150 keV and reprocessing features. This spectral form can be interpreted as being due to an accretion disk corona (ADC) (Dove et al. 1997 and references therein).

The short-term variability of the X-ray emission has been studied in order to gain better insight into the physical processes at work near the compact object. Cyg X-1 was the first source for which X-ray variability on timescales $<$1 s was detected (Oda et al. 1971). For a long time this variability was suspected to be a special black hole signature, but today we know that X-ray binaries containing a neutron star instead of a black hole can display similar behavior (Stella et al. 1985). Nevertheless, the efforts in trying to identify a BHC by its irregular short-term variability are continuing (van der Klis 1995).

Until now, no special process could be determined that describes all the properties of the observed short-term variability. We define "variability on short timescales" as variability faster than a few 100 s, with emphasis on timescales $<$1 s. These rapid fluctuations are usually described in terms of shot noise models. It has become clear, however, that in the framework of applying conventional shot noise models, complex shot profiles or distributions of shot durations and amplitudes have to be assumed to explain the observations (Nolan et al. 1981; Lochner et al. 1991; Negoro et al. 1994). Shot noise processes exhibit a fixed dynamical behavior in the sense that if the shots are given, no new dynamical information is produced during the run of the Poisson distributed point process. Only by the summation of individual shots the temporal correlations in the time series of the process are generated (Sect. 2.3).

We use the alternative method of applying Linear State Space Models (LSSMs) which are based on stochastic processes (i.e. autoregressive (AR) processes, Scargle 1981) to describe the time series variability. In this case the dynamics of the process are produced using a different approach: each value of the time series refers to earlier values, with their temporal correlation being determined by the dynamical parameters of the system (Sect. 3.1).

The time series of a standard shot noise (exponential decay with one relaxation timescale) and an AR process of first order might look very similar, although the underlying processes differ. The similarity in the time domain leads to shot noise and AR processes both exhibiting an exponentially decaying auto-

Send offprint requests to: K. Pottschmidt, (katja@astro.uni-tuebingen.de)

correlation function (König & Timmer 1997). In contrast to the similarity of the time series, however, the theoretical frequency spectra are different (cf. Eq. 4 and 8). Whereas shot noise profiles with varying relaxation timescales have to be added to approximate the observed periodogram (Lochner et al. 1991), only one dynamical AR parameter is needed to reproduce its properties (Sect. 3.3 and 4.1).

We have studied the high time resolution EXOSAT ME lightcurves of Cyg X-1. The data are presented in Sect. 2.1. A commonly used method to analyze X-ray variability is to work in the frequency domain by fitting theoretical power spectra to the periodogram of a lightcurve: The periodogram of Cyg X-1 and the power spectra of the usually applied shot noise models are reviewed in Sect. 2.2 and 2.3, respectively. Our analysis of the lightcurves with LSSMs, however, is not based on fitting the periodogram but on an alternative procedure working in the time domain. Sect. 3 deals with the theory of the LSSM analysis. Our results are presented in Sect. 4, and in Sect. 5 a possible explanation for the derived relaxation timescale is discussed combining the temporal LSSM results and simulations of comptonized radiation using an accretion disk corona model for Cyg X-1.

2. The short-term X-ray variability of Cyg X-1

2.1. The data

The EXOSAT raw data have been stored on *Final Observation Tapes* (FOTs) and are now available at the *HEASARC* archive. Table 1 lists the FOT observations of Cyg X-1 that we have analyzed with Linear State Space Models. We have chosen the ME datastreams provided by the primary timing telemetry modes HTR3 und HER6. These observations only contain events registered in the Argon counters (1–20 keV). The lightcurves are given as countrates normalized to one half of the detector array (i.e. four Argon counters). Using the *Interactive Analysis* (IA) software, we extracted lightcurves corrected for dead-time effects and collimator efficiency (for an overview of the IA see Parmar et al. 1995). For the purpose of this paper an explicit background subtraction is not necessary since the LSSM is implicitly modeling the measurement process (see Sect. 3.2, Eq. 7).

All EXOSAT observations of Cyg X-1 have found the source in its usual hard state. An example for the characteristic hard state variability of Cyg X-1 on short timescales can be seen in Fig. 1.

2.2. The periodogram of Cyg X-1

The periodogram $P(f_k)$ of a lightcurve $y(t_j)$ (where $j = 1,\ldots,N$) is providing the "strength" of harmonic variations with a certain frequency f_k in the lightcurve. $P(f_k)$ is defined as the squared modulus of the discrete Fourier transform of $(y(t_j) - \bar{y})$ and is calculated for the Fourier frequencies

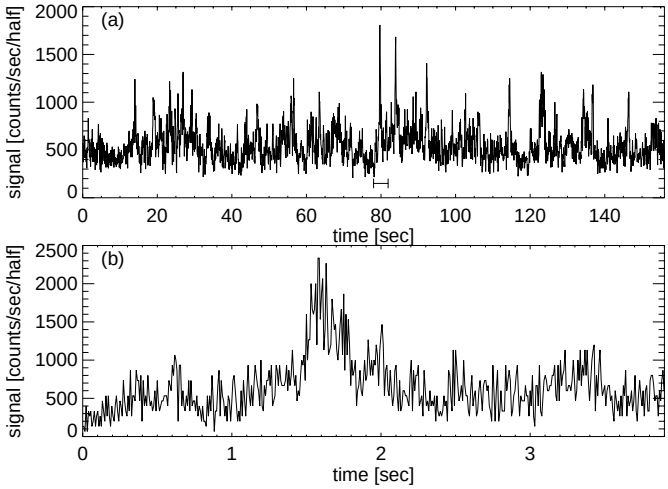

Fig. 1. a X-ray lightcurve of Cyg X-1, showing a part of the fifth observation on FOT Nr. EE8087 (No. 1 of Table 1, energy range=1–20 keV, bin time=62.4 ms, length=156 s). **b** Blow-up of the marked segment of subfigure a with a length of 3.9 s and the original bin time of 7.8 ms, showing a typical shot structure. Both lightcurves are plotted without error bars for reasons of clarity.

Table 1. EXOSAT ME observations that have been analyzed with LSSMs.

No.	FOT tape [a]	start time (UT) [dd.mm.yy hh:mm]	original time resolution [ms]
1	EE8087(05)*	28.07.83 22:51	07.813
2	EE1723(06)*	25.09.83 05:15	01.953
3	EE2461(06)	21.05.84 04:59	07.813
4	EE2956(06)	07.07.84 10:57	15.630
5	EE2956(07)	07.07.84 13:23	15.630
6	EE2929(10)	09.07.84 14:59	11.720
7	EX3620(08)*	24.07.84 20:20	07.813
8	EE3962(13)	02.11.84 19:20	09.766
9	EE3962(16)	02.11.84 20:27	11.720

[a] Final observation tape number and number of observation therein (*: telemetry mode HTR3, else: HER6).

$f_k = k/(N\cdot\Delta t)$ with bin time Δt and $k \in \{1,\ldots,M\}$, where M is the integer part of $N/2$ (Scargle 1982):

$$P(f_k) = \frac{1}{N}\left|\sum_{j=1}^{N}(y(t_j)-\bar{y})e^{2\pi i f_k t_j}\right|^2 \qquad (1)$$

Fig. 2 shows the logarithmically plotted sample periodogram (solid line) of the observation No. 1 (Table 1). It has been obtained by averaging over periodograms $P(f_k)$ from 48 different lightcurve segments (details see caption of Fig. 2). Since $P(f_k)$ is a χ^2_2-distributed random variable, its standard deviation is equal to its mean (van der Klis 1989). Therefore, an individual periodogram exhibits large fluctuations (Fig. 2, dots). Calculating the sample periodogram significantly reduces the scatter and allows the possibility to estimate the theoretical spectrum of the process responsible for the observed variability.

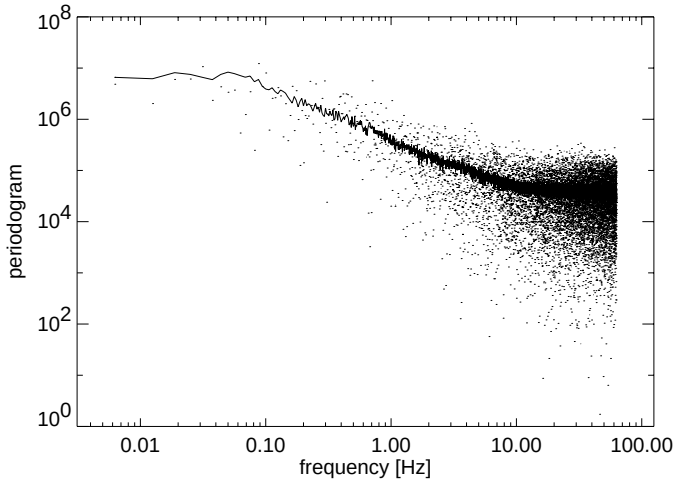

Fig. 2. Sample periodogram (solid line) of Cyg X-1, averaged over 48 individual periodograms, which have been obtained by dividing the original lightcurve (No. 1, Table 1) into 48 segments of 156 s each and calculating $P(f_k)$ for each segment (Eq. 1). The values of a typical individual periodogram, fluctuating wildly, are also displayed (dots).

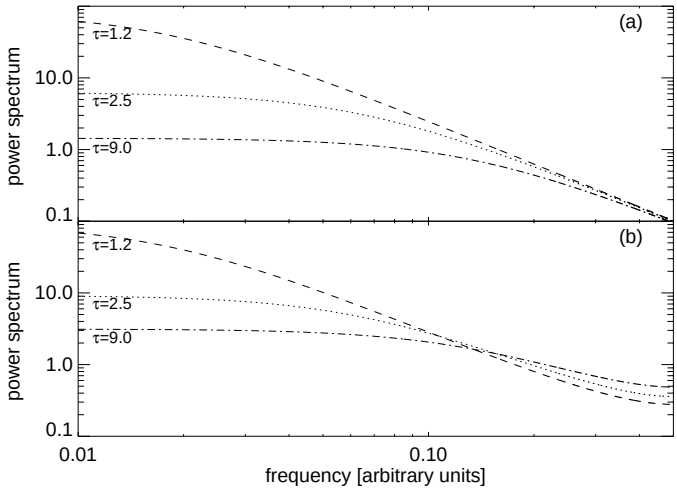

Fig. 3. a Shot noise power spectra for three different values of τ, calculated according to Eq. 4 (λ=1, h_0=1). **b** LSSM power spectra for the same values of τ as in (**a**), calculated according to Eq. 8 (σ_ϵ^2=1). All power spectra are given in arbitrary units and Δt has been normalized to 1. In subfigure b, the variance of the observation-noise, σ_η^2, has been set to 0 to allow direct comparison of **a** and **b**.

The periodogram of the short-term variability of Cyg X-1 in its hard state is well known and exhibits the following distribution of timescales (Fig. 2):

- For frequencies above 10 Hz white noise dominates the periodogram which means that the variability of the lightcurves on all corresponding timescales is almost equally strong. These fluctuations (i.e. photon statistics, particle background) are introduced by the measurement procedure. It is common practice to subtract a constant (corrected for deadtime effects) which represents this noise component from the periodogram (Belloni & Hasinger 1990b; Zhang et al. 1995).
- Towards lower frequencies the power of the variability increases within the frequency range of roughly 0.04–10 Hz. This behavior is called red noise. It is often modeled by a power law, $f^{-\alpha}$. Variability of the $f^{-\alpha}$-type is known from many X-ray binaries (van der Klis 1995) and also from active galactic nuclei (McHardy 1989). In the case of Cyg X-1, α is approximately 1 (Nolan et al. 1981; Lochner et al. 1991).
- An important feature indicating the stationarity of the short-term variability process is the flattening of the power spectrum for frequencies below ≈0.04 Hz. This flat top corresponds to the absence of additional long-term variations in the lightcurves. There are, however, some EXOSAT ME observations of Cyg X-1 which show low frequency noise in the form of increasing power towards lower frequencies below 0.001 Hz (Angelini et al. 1994). Since this component is not always present, it is most likely not produced in the same physical process as the short-term variability. Suggested causes for this low frequency variabilities are instabilities in the mass transfer process. Sometimes the low frequency noise is associated with absorption dips in the lightcurve (Kitamoto et al. 1984; Angelini et al. 1994).
- Several authors reported a transient quasi-periodic oscillation (QPO) feature in the power spectrum with a central frequency of about 0.04 Hz (Kouveliotou et al. 1992; Angelini et al. 1994; Vikhlinin et al. 1994; Borkus et al. 1995), whereas other authors have not found any evidence for QPOs (Belloni & Hasinger 1990b; Miyamoto et al. 1992). Thus the significance of this feature is not yet clear. In Fig. 2 no QPO feature is present.

2.3. The shot noise model

Terrell (1972) proposed that the structures observed in the lightcurves of Cyg X-1 might be due to a shot noise process $s(t)$, i.e. the superposition of randomly occuring shots with the shot profile $h(t')$:

$$s(t) = \sum_i h(t - t_{\rm SH}) \tag{2}$$

Here the $t_{\rm SH}$ are the times at which the shots occur, with the time intervals between the $t_{\rm SH}$ following a Poisson distribution.

The standard shot profile $h(t')_{\rm ST}$ is identical for all shots and consists of an instantaneous rise to height h_0 and an exponential decay with the decay time τ:

$$h(t')_{\rm ST} = \begin{cases} 0 & ,t' < 0 \\ h_0 \cdot e^{-t'/\tau} & ,t' \geq 0 \end{cases} \tag{3}$$

Shot noise models are often evaluated by comparing their theoretical power spectrum to the observed power spectrum (Belloni & Hasinger 1990b; Lochner et al. 1991). The theoretical power spectrum of the standard shot noise process is (Lehto 1989):

$$S(f)_{\rm SN} \propto \frac{\lambda {h_0}^2}{(1/\tau)^2 + (2\pi f)^2}, \quad f \neq 0, \tag{4}$$

where $1/\lambda$ is the average time interval between the shots. $S(f)_{\rm SN}$ provides the flat top for $f \ll 1/(2\pi\tau)$ but has a fixed logarithmic slope of $\alpha = 2$ for higher frequencies (Fig. 3a). Since the shot noise process $s(t)$ is continuous in t, whereas the observed lightcurve is the result of integrating the measured counts over a finite number of intervals Δt, $S(\omega)_{\rm SN}$ must be corrected for binning. Lochner et al. (1991) have shown, that binning makes the shot noise power spectrum even steeper for high frequencies.

Neither the observed slope nor the white noise floor of the Cyg X-1 periodogram (Fig. 2) can be reproduced by the standard shot noise process. In frequency domain fits the white noise level is usually treated as an additional constant parameter (cf. Sect. 2.2). To model the observed slope, different shot profiles with distributions of shot durations and shot amplitudes have been proposed. A number of those models, each having many degrees of freedom, are able to reproduce the observed periodogram and other second order statistics (Belloni & Hasinger 1990b, Lochner et al. 1991). Higher order statistics like the time skewness (Priedhorsky et al. 1979) or phase portraits (Lochner et al. 1991) were also studied but no special shot noise model could be singled out that allows for a homogeneous description of different observations. In Sect. 3.3 we discuss the theoretical power spectrum of a first order LSSM and show that it can reproduce all the features of the hard state periodogram of Cyg X-1, requiring only one temporal parameter τ (Fig. 3b).

3. The Linear State Space Model (LSSM)

The LSSM analysis is a recently developed tool to model stochastic time series (Gantert 1993). It has e.g. been used to describe medical time series (hand-tremor data,Timmer 1995). König & Timmer (1997) were the first to apply the new method to astronomical data by successfully fitting lightcurves of active galactic nuclei with first order LSSMs (see also König et al. 1997). The mathematical background of the LSSMs and the associated fitting-procedure have been discussed in detail by König & Timmer (1997) and in the references therein. Here, we shall concentrate on first order LSSMs, for we found them to be appropriate to describe the Cyg X-1 lightcurves (see Sect. 4).

3.1. The autoregressive process

One possibility to model irregular variability (i.e. temporal variations that cannot be forecasted exactly) is to assume that it is caused by a chaotic process (Voges et al. 1987; Unno et al. 1990). The LSSMs, on the other hand, are based on the alternative assumption, that the variability of the observed system is produced by a stochastic process. The LSSMs use the rather general autoregressive (AR) formulation for the stochastic system-lightcurve $x(t_j)$.

The AR processes were first introduced by Yule (1927) to model the variability of Wolf's sunspot numbers and have been well studied since then (e.g. by Scargle 1981). An *AR process of order* p (AR[p]) is defined by:

$$x(t_j) = \sum_{i=1}^{p} a_i \cdot x(t_j - i \cdot \Delta t) + \epsilon(t_j),\ \epsilon(t) \propto \mathcal{N}(0, \sigma_\epsilon^2) \quad (5)$$

The time series $x(t_j)$ is sampled at discrete times t_j with time resolution Δt. The purely stochastic component $\epsilon(t)$, is a Gaussian random variable with mean 0 and variance σ_ϵ^2. Since Eq. (5) is of the same structure as a regression equation for the variables $x(t_j)$ and $(x(t_j - i \cdot \Delta t))$ the name *autoregressive* process has been assigned to it.

In an AR lightcurve, for each t_j the value of the random variable $x(t_j)$ is correlated with the values of the process at earlier times. This correlation is decreasing with increasing time differences between two lightcurve values (expressed by an exponentially decaying autocorrelation function). The stochastic component $\epsilon(t)$ is the reason that the process does not simply come to rest. $\epsilon(t)$ is an intrinsic property of the system-variability: the system-noise.

The temporal correlations in the AR lightcurve are characterized by the dynamical parameters (a_i). The p dynamical parameters are related to p temporal parameters, describing the temporal structures in the lightcurves: depending on the process, the (a_i) represent stochastic relaxators with relaxation times τ, or damped stochastic oscillators with relaxation times τ and periods P, or both (Honerkamp 1994). In case of an first order AR process there is only one dynamical parameter $a_1 = a$. For stationary processes $|a|$ must be <1 and only positive values of a lead to plausible physical models. The corresponding temporal parameter, $\tau = -1/\ln|a|$, is the relaxation time of a stochastic relaxator, one representation of which is an exponentially decaying shot as described by Eq. (3).

3.2. The observation-noise

For the determination of the temporal parameters of the system-process the noise which is caused by the measurement (i.e. photon statistic, particle background) has to be considered because it disturbs the temporal structures of the system-lightcurve. If the observation of a system-lightcurve is modeled with a plain AR process, the so called observation-noise will lead to an underestimation of the true temporal system-parameters (Robinson & Nather 1979; König & Timmer 1997). In order to solve this general problem, a LSSM consists of two equations: the system-equation for the intrinsic system-lightcurve and the observation-equation for the measured lightcurve. The latter describes the observed lightcurve $y(t_j)$ by *explicitly considering the influence of the observation-noise* $\eta(t_j)$ on the system-lightcurve.

The important model for the analysis of the short-term variability of Cyg X-1 is the *LSSM of first order*:

$$x(t_j) = a \cdot x(t_j - \Delta t) + \epsilon(t_j), \quad \epsilon(t_j) \propto \mathcal{N}(0, \sigma_\epsilon^2) \quad (6)$$

$$y(t_j) = c \cdot x(t_j) + \eta(t_j), \quad \eta(t_j) \propto \mathcal{N}(0, \sigma_\eta^2) \quad (7)$$

Like the system-noise $\epsilon(t_j)$, the observation-noise $\eta(t_j)$ is modeled by a Gaussian noise component; c is a constant normaliza-

tion factor. The equations for higher order LSSMs are given by König & Timmer (1997) (the temporal parameters of an LSSM of order p (LSSM[p]) correspond to the p dynamical parameters of Eq. 5).

3.3. The power spectrum

The power spectrum $S(f)_{\mathrm{LSSM[1]}}$ of a first order Linear State Space Model has the following form (König & Timmer 1997):

$$S(f)_{\mathrm{LSSM[1]}} \propto \frac{\sigma_\epsilon^2}{1 + a^2 - 2\,a\cos(2\pi f)} + \sigma_\eta^2 \qquad (8)$$

The examples for $S(f)_{\mathrm{LSSM[1]}}$ displayed in Fig. 3b show the flat top as well as red noise. The observational white noise floor is also provided by Eq. 8 but has been omitted in Fig. 3b ($\sigma_\eta^2 = 0$) to allow the direct comparison with the standard shot noise spectra (Fig. 3a): In contrary to the fixed red noise slope $\alpha = 2$ of the standard shot noise spectra, the slope of $S(f)_{\mathrm{LSSM[1]}}$ can be modeled by adjusting a, i.e. τ. All the features of the hard state power spectrum of Cyg X-1 can thus be reproduced by the power spectrum of the LSSM[1] which is defined by only one temporal parameter $\tau = -1/\log|a|$. Furthermore, Eq. 8 does not need to be corrected for binning effects, since the definition of the LSSM already is discrete in t (see Eq. 6 and 7).

Principally, LSSMs can be evaluated by fitting their power spectra to the measured periodogram. However, fits in the frequency domain do not allow the explicit modeling of the observational noise and may be influenced by several other sources of uncertainties, especially by spectral leakage, which contaminates the power spectrum of each finite time series (Deeter & Boynton 1982; Deeter 1984). To avoid these uncertainties our LSSM analysis was performed in the time domain by direct comparison of the model-lightcurves and the measured lightcurves. This method allows fits with a statistical significance higher than that of the frequency domain fits (König & Timmer 1997).

3.4. The fitting procedure

The parameters of a LSSM[p] fit are estimated with the help of the maximum likelihood procedure: the set of parameters is derived, for which the probability of observing the measured lightcurve $y(t)$ is at maximum. We have obtained those parameters using the expectation-maximization (EM) algorithm (Honerkamp 1994). The method is iterative, starting from a set of initial parameter values. In the expectation step, the Kalman filter is applied, which allows to estimate the unobservable system-lightcurve $x(t_j)$ by using the observed lightcurve $y(t_j)$ and a given set of LSSM parameters. In the following maximization step the likelihood function is maximized, taking the estimated $x(t_j)$ into account and providing a new set of parameters. The results of this iterative procedure are best estimates for the LSSM[p] parameters and for the intrinsic system-lightcurve (a detailed example is discussed in Sect. 4.1). Note, that the latter is *not* produced using a smoothing filter: all variability timescales of the observed lightcurve (see e.g. Fig. 4a) are still present in the derived system-lightcurve (see e.g. Fig. 4b).

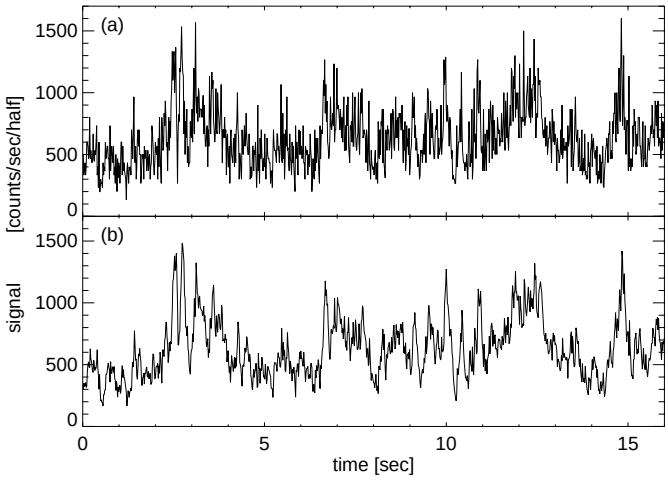

Fig. 4. a One of the 900 EXOSAT ME Cyg X-1 lightcurves with a length of 16 s and a bin time of 16 ms, which were modeled by LSSMs. Mean countrate: 633.1 counts/sec/half, standard deviation: 234.5 counts/sec/half. **b** Best estimate for the autoregressive system-lightcurve, which has been obtained by applying a LSSM of order $p = 1$ to the lightcurve displayed above (see Table 2). Both lightcurves are shown without error bars for reasons of clarity.

The length and the time resolution of lightcurves, which are analyzed by LSSMs, have to be chosen considering the following requirements:

- The duration of the lightcurve has to be several times the relaxation timescale, which is expected to be a few tenths of a second (shot noise models), or the relaxator cannot be found.
- The bin time has to be well below the relaxation timescale to allow us to distinguish the relaxator from statistical fluctuations.

Simulations by König (1997) have shown that the duration should be at least 5 times larger and that the bin time should be at least 10 times smaller than τ. In order to fulfill these criteria without an unreasonable increase in LSSM computing time, we have fitted lightcurves with a bin time of 16 ms and length of 16 s (e.g. Fig. 4a). Although this time interval is shorter than the intervals typically studied in the context of shot noise analysis, it is long enough for the determination of the relaxator.

4. Results

4.1. LSSM fits of various order to one exemplary lightcurve

Table 2 shows the results of LSSM fits of order 0–5 to the lightcurve segment displayed in Fig. 4a: The relaxation timescale τ of about 0.2 s, which is derived by the LSSM[1] fit, is also found by the fits of higher order (the LSSM[0] represents uncorrelated white noise and therefore does not yield a temporal parameter). All other temporal correlations are decaying within a few time

Table 2. Results of LSSM fits of various order to the lightcurve in Fig. 4a.

Order p of the LSSM	Relaxator τ [s]	Period P [s]	KS probability %
0	-	-	0.0
1	0.185	-	93.5
2	0.209	-	87.0
	0.018	-	
3	0.177	-	97.6
	0.022	0.092	
4	0.204	-	88.5
	0.046	0.128	
	0.011	-	
5	0.175	-	97.4
	0.046	0.128	
	0.015	0.096	

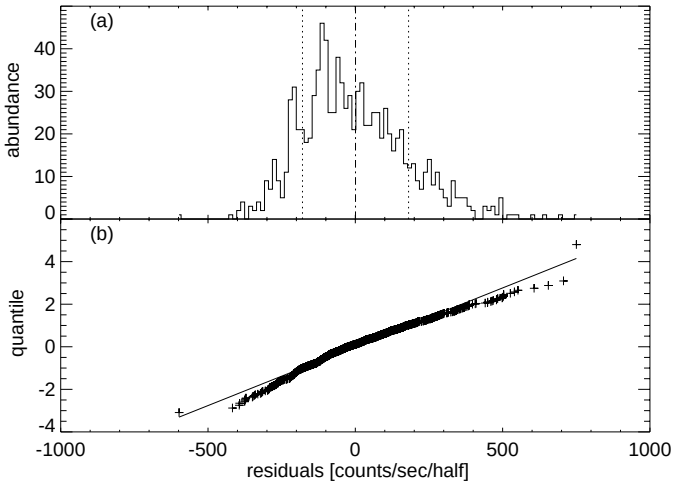

Fig. 5. a Distribution and **b** normal quantile plot of the residuals of the LSSM[1] fit to the lightcurve given in Fig. 4a. The lines in subfigure a indicate the mean and standard deviation of the observation-noise. The straight line in subfigure b corresponds to a Gaussian distribution having the same mean and variance as the distribution of the residual lightcurve.

bins. Since they are due to statistical fluctuations they are negligible (König 1997). This means, that the dynamics of the lightcurve can most likely be described by one relaxation timescale. If this is the case, the LSSM[1] fit should deliver an adequate description of the observed lightcurve and the goodness of fit should not increase significantly for higher order LSSMs.

A statistical test on the residuals, i.e. the difference between the derived system-lightcurve and the observed lightcurve, was performed to determine the quality of the LSSM fits: If a given LSSM can describe the observation, the residuals should be an uncorrelated white noise realization (Eq. 7). In this case all the temporal correlations of the observed lightcurve are modeled by the system-lightcurve. We use the Kolmogorov-Smirnov (KS) test to quantify the goodness of the LSSM fits. It compares the power spectrum of the residuals to a flat white noise power spectrum.

In Table 2 we list the KS probabilities for the residual lightcurves to actually be white noise realizations. For the LSSM[1] fit a very high probablity of 93.5% is reached, which means that the observed lightcurve can be well modeled by an LSSM[1] process. This is consistent with the visual impression from Fig. 4: the LSSM[1] estimate (b) tracks the observed lightcurve (a) very closely. Higher order LSSM fits do not improve the fit significantly. The LSSM[0] (white noise) is of course rejected at any level of confidence.

The distribution of the LSSM[1] model residuals is shown in Fig. 5a. Its mean and variance are 0.7 counts/sec/half and (179.9 counts/sec/half)^2, respectively. Thus the variance of the observation-noise is about 82% of the upper limit as given by the mean countrate of the original lightcurve and assuming a pure Poisson process. The lower half of Fig. 5 displays the normal quantile plot of the fit residuals: it arranges the residuals in increasing order and for each data value indicates the position that corresponds to the same probability in a normal distribution. If the data are normally distributed, all points should lie on a straight line. Fig. 5b shows that the distribution of the residuals can be approximated by a Gaussian distribution, but is compressed for low and stretched for high countrates. This indicates that the fit residuals are Poisson-distributed as expected for the observation-noise (mean countrate of the original lightcurve: 10.1 counts per 16 ms time bin). The LSSM[1] model parameters reflect the Poisson distribution of the observation-noise by underestimating the Gaussian variance σ_η^2 given as (143.8 counts/sec/half)^2 in this example.

4.2. LSSM fits of first order to a sample of lightcurves

In order to obtain a reliable value for the temporal parameter τ, we have fitted LSSM[1]s to a sample of 900 lightcurve segments covering a total length of four hours. We have used 1600 s of each of the nine observations listed in Table 1. The 1600 s consist of 100 equally long, uninterrupted segments with a temporal resolution of 16 ms.

For each of the nine observations 100 values for the relaxator τ were obtained. In Table 3, the mean $\bar{\tau}$, the standard deviation s_τ, and the most probable value $\tau_{\max}$ of these distributions are listed. Averaging $\bar{\tau}$, s_τ, and $\tau_{\max}$ over the nine observations gives (0.28±0.04) s, (0.13±0.03) s, and (0.19±0.03) s, respectively. All distributions exhibit the same asymmetric form, in the sense that $\tau_{\max}$ is always lower than $\bar{\tau}$ but still higher than the 1σ deviation. This kind of distribution is consistent with the results that have been obtained from simulations of AR lightcurves based on one temporal parameter τ (Hamilton & Wu 1987).

The lightcurves of three of the observations (No. 1, 2, and 7 of Table 3) take the whole Argon energy range (1–20 keV) into account, i.e. their absolute countrates may be compared. Even though the analyzed segments of one of those three observations (No. 7) have a considerably smaller mean countrate than those of the other two, the corresponding distribution of τ is not significantly different. This means that no correlation between τ and the luminosity can be seen, which is confirmed

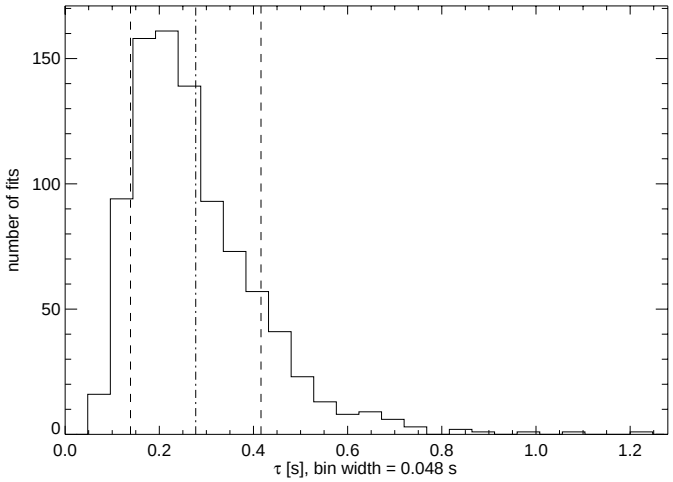

Fig. 6. Distribution of values of the relaxation timescale τ, obtained from LSSM[1] fits to a sample of 900 Cyg X-1 lightcurves. The mean value of the distribution is $\bar{\tau} = 0.28\,\mathrm{s}$ (dash-dotted line) with the standard deviation $s_\tau = 0.14\,\mathrm{s}$ (dashed lines). The most probable value is $\tau_{\max} = 0.22\,\mathrm{s}$.

within each of the nine observations: the mean countrates and the relaxation times of the 100 segments are not correlated.

Since the observations provide consistent results, all 900 values for τ can be combined, in order to arrive at a distribution with better statistics (Fig. 6). Note, that this non-Gaussian distribution, resulting from the maximum likelihood estimation of τ, cannot be described analytically (Hamilton & Wu 1987). In addition, simulations have shown that the distribution of τ is contaminated by bad fit results at its "high τ end" due to numerical effects (Hamilton & Wu 1987; König 1997). Therefore, $\bar{\tau}$ can be expected to overestimate the "true" relaxation timescale of Cyg X-1, whereas the most probable value $\tau_{\max}$ should be a better estimator.

5. Summary and discussion

5.1. The LSSM[1] results — a generalization of the shot noise approach

We have shown that the short-term variability of the EXOSAT ME lightcurves of Cyg X-1 can be well described by a Linear State Space Model of first order, i.e. the dynamics of the system can be modeled as an autoregressive process with one temporal parameter – the relaxation timescale τ. We find τ to be $(0.19\pm0.03)\,\mathrm{s}$ for the ME energy-range. The relaxator is not found to be correlated either with time nor with the luminosity of the source, indicating that the physical process producing the emitted radiation is very stable and suggesting that the short-term variability is independent of the mass accretion rate of the system. The LSSM analysis in the time domain allows us to estimate the fraction of the countrate that is due to observation-noise. When analyzing the periodogram in the frequency domain this white noise component can only be represented by a constant whose extraction is not trivial (Belloni & Hasinger 1990a; Zhang et al. 1995). Furthermore, the problem of spectral leakage that has to be delt with in the frequency domain, is circumvented by fitting in the time domain. For these reasons our LSSM analysis delivers results with higher statistical significance than corresponding frequency domain fits (König & Timmer 1997).

Table 3. Results of the LSSM(AR[1]) fits to EXOSAT ME observations of Cyg X-1.

No. [a]	energy channels	count-rate [b]	$\bar{\tau}$ [s]	s_τ [s]	$\tau_{\max}$ [s]
1	1–128	565±57	0.26	0.10	0.22
2	1–128	567±37	0.36	0.17	0.22
3	9–21, 22–51	541±33	0.30	0.16	0.22
4	5–19, 27–65	388±19	0.26	0.12	0.17
5	5–16, 27–65	457±29	0.31	0.16	0.19
6	7–21, 26–81	499±35	0.25	0.11	0.17
7	1–128	389±24	0.25	0.09	0.22
8	5–16, 17–49	359±14	0.27	0.14	0.17
9	5–16, 17–49	321±14	0.24	0.11	0.17

[a] Number of the observation following the notation of Table 1; [b] Average over the mean countrates of the 100 lightcurve segments and its standard deviation ([counts/sec/half]).

These LSSM[1] results allow a much simpler description of hard state short-term variability than multi-timescale shot noise models. Although a detailed quantitative comparison is beyond the scope of this paper, the reproduction of the periodogram by the LSSM[1] (compared to its approximation by adding shot-profiles with different timescales, corrected for observation-noise and binning) as well as the greater sensitivity of the LSSM fitting procedure (compared to frequency domain fits, which are usually used to evaluate shot noise models) suggest that LSSM[1]s are better suited to describe the nature of the observed variability.

The LSSMs can model the different realizations of a stochastic relaxator τ, whereas shot noise models are generally restricted by the definition of special shot forms. Shot noise lightcurves therefore might be regarded as a subclass of LSSM lightcurves in the sense that a superposition of exponentially decaying shots can be interpreted as *one* possible realization of an intrinsic AR[1] process. The inspection of the measured lightcurves of Cyg X-1 implies that the source of the derived AR[1] process is indeed the stochastic superposition of individual shot events, corresponding to the basic idea of shot noise. We note that on larger timescales this kind of variability is also present in the X-ray emission of active galactic nuclei (AGN) (e.g. McHardy 1989; Mushotzky et al. 1993; König & Timmer 1997; König et al. 1997). The physical mechanism responsible for such a temporal behavior, however, is not yet understood.

5.2. The LSSM results in the light of time-dependent comptonization models

Recently, the discussion concerning accretion physics has begun to concentrate on the consideration of timing and spectral prop-

erties of the X-ray emission as two aspects of the same model (Kazanas et al. 1997; König et al. 1997; Wilms et al. 1997; and references therein). The spectrum of both, AGN and the hard state of galactic black hole candidates, is usually explained by inverse Comptonization, where soft X-ray photons, provided by a cold accretion disk, are upscattered by inverse Compton collisions in a hot plasma to produce the observed high energy power-law.

In this context it can be assumed that the observed X-ray temporal behavior is the result of the processing of short shots of seed photons within the accretion disk corona (Payne 1980). The initial photon pulse is hardened and temporally broadened while diffusing through the corona. As harder photons in the emerging spectrum have, on average, undergone more scattering events, they have stayed in the corona for a longer time than softer photons and the emerging pulse is comparatively broader (observed in AGN by König et al. 1997). In addition, variability structures in high energy lightcurves exhibit a characteristic time-lag with respect to those in low energy lightcurves (Fig. 7). Frequency-dependent time-lags have e.g. been observed in Ginga and RXTE observations of Cyg X-1 (Miyamoto et al. 1988; Miyamoto et al. 1992; Wilms et al. 1997). The question to what extent these lags are produced in a hot corona or wether they are intrinsic properties of the cold disk is still unresolved (Miyamoto et al. 1988; Miller 1995; Nowak & Vaughan 1996; Nowak et al. 1998). Nowak et al. (1998), however, show that the frequency-dependent time-lags of Cyg X-1 can be qualitatively reproduced using a simple propagation model (but they also point out that the longest observed time-lags ($\approx$0.1 sec) can probably not be explained by Comptonization). Another challenge for combined spectral and temporal theories is given by modeling the coherence of variability structures in different energy bands which is observed to be near unity over a large frequency range in Cyg X-1 (Vaughan & Nowak 1997; Wilms et al. 1997).

Additional support for the time-dependent Comptonization model comes from the joint spectral and temporal analysis of AGN, which have similar properties to those of Cyg X-1. For a sample of AGN observations we were able to show that a linear correlation between the photon index Γ and the LSSM[1] timescale τ exists, in the sense that harder spectra have a longer variability timescale (König et al. 1997). By comparing the observed Γ-τ relation with Monte Carlo simulations of time-dependent Comptonization models, it is possible to scale the model geometry (König 1997). For the hard-state galactic black hole candidates a similar study cannot be performed since not enough objects are known. What can be done, however, is to check whether our best-fit LSSM models for Cyg X-1 could, at least roughly, be explained with a time-dependent Comptonization model.

We have computed shot profiles for several possible accretion geometries using a linear Monte Carlo code. The detailed results of these simulations will be discussed elsewhere. Since shot noise can be regarded as a special representation of an AR[1] process (see Sect. 5.1), we can use the computed shots to generate lightcurves based on these profiles, including an additional white noise component. In analogy to our treatment of the distribution of τ seen in the observations, we derive a most probable value for τ from the simulated lightcurve samples, $\tau_{\rm th}$. We find $\tau_{\rm th} = (3 \ldots 6) R_{\rm c}/c$, with $R_{\rm c}$ being the radius of the corona. The profile of a Compton-shot only depends on the relative size of the system, parameterized by the light travel time through one radius of the spherical corona, R_c/c. By identifying $\tau_{\rm th}$ with the measured value of $\tau = 0.19$ s, it is therefore possible to express the measured τ in terms of the coronal radius. Our simulations give a first estimate of 320–640 Schwarzschild radii for the coronal radius (assuming a mass of $10 M_\odot$ for the black hole). Other authors estimate the size of the Comptonization cloud in the hard state to be $\approx$100 Schwarzschild radii (Esin et al. 1997, ADAFs) or $\approx$23 Schwarzschild radii (Nowak et al. 1998, from minimal time-lags). These values are only in rough agreement and a better understanding of the relation between spectral and temporal properties is needed to arrive at a consistent picture. We plan a more detailed study of the Compton-shot profiles as well as LSSM analyses of RXTE data to further constrain the accretion geometry of Cyg X-1.

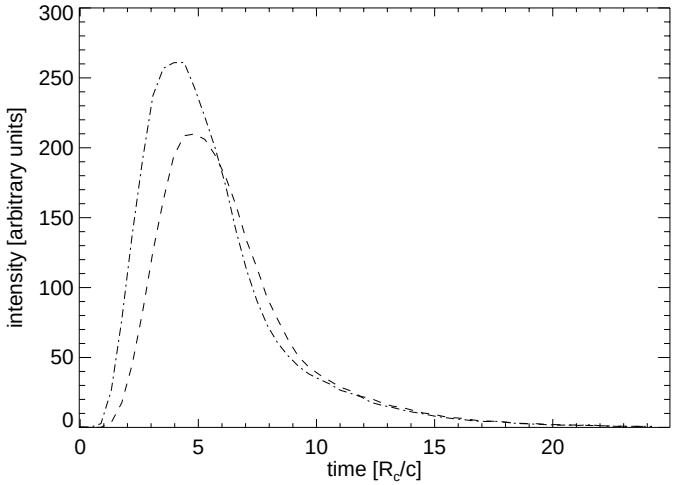

Fig. 7. Shot profiles for the energy-ranges 4–5 keV (dash-dotted line) and 12–23 keV (dashed line). The profiles have been computed for an accretion disk corona (ADC) model with an accretion geometry as described by Dove et al. (1997). This geometry is similar to an advection dominated flow (ADAF, Abramowicz et al. 1995; Narayan 1996). The ADC model parameters were chosen to be appropriate for Cyg X-1 (disk temperature: $kT_{\rm d}$=200 eV, coronal temperature: $kT_{\rm c} = 66$ keV, optical depth of the corona: $\tau_{\rm c} = 2.1$; Dove et al. 1997).

Acknowledgements. We thank J. Timmer for his assistance concerning the LSSM analysis method and C. Gantert for writing the LSSM code which has been kindly provided from the "Freiburger Zentrum für Datenanalyse und Modellbildung". We thank M. Nowak and J. Dove for useful discussions as well as S. Kitamoto, the referee, for helpful comments. This research has made use of data obtained through the HEASARC Online Service, provided by NASA-GSFC.

References

Abramowicz M., Chen X., Kato S., et al., 1995, ApJ 438, L37

Angelini L., White N.E., Stella L., 1994, in Makino F., Ohashi T. (eds.) New Horizon of X-Ray Astronomy. Universial Academy Press, Tokyo, 429
Belloni T., Hasinger G., 1990a, A&A 230, 103
Belloni T., Hasinger G., 1990b, A&A 227, L33
Bolton C.T. 1972, Nat 235, 271
Borkus V.V., Kaniovsky A.S., Efremov V.V., et al., 1995, Astron. Let. 21, 794, (PAZh, 21, 883)
Bowyer S., Byram E.T., Chubb T.A., Friedman H., 1965, Sci 147, 394
Cui W., Zhang S.N., Jahoda K., et al., 1997, in Winkler C., Courvoisier T.J.-L., Durouchoux P. (eds.) The Transparent Universe, ESA SP-382. ESA Publications Division, Noordwijk, 209
Deeter J.E., 1984, ApJ 281, 482
Deeter J.E., Boynton P.E., 1982, ApJ 261, 337
Dove J.B., Wilms J., Maisack M., Begelman M.C., 1997, ApJ 487, 759
Esin A.A., Narayan R., Cui W., et al., 1997, ApJ, submitted (astro-ph/9711167)
Friend D.B., Castor J.I., 1982, ApJ 261, 293
Gantert C., 1993, Dissertation, Albert-Ludwigs-Universität, Freiburg im Breisgau
Hamilton D., Wu K.H., 1987, J. Time Ser. Anal. 16, 249
Herrero A., Kudritzki R.P., Gabler R., et al., 1995, A&A 297, 556
Hjellming R.M., Wade C.M., 1971, ApJ 168, L21
Honerkamp J., 1994, Stochastic Dynamical Systems: Concepts, Numerical Methods, Data Analysis. VCH, Weinheim
Kazanas D., Hua X.-M., Titarchuk L., 1997, ApJ 480, 735
Kitamoto S., Miyamoto S., Tanaka Y., et al., 1984, PASJ 36, 731
König M., 1997, Dissertation, Eberhard-Karls-Universität Tübingen
König M., Timmer J., 1997, A&AS 124, 589
König M., Staubert R., Wilms J., 1997, A&A 326, L25
Kouveliotou C., Finger M.H., Fishman G.J., et al., 1992, IAU Circ. 5576
Lehto H.J., 1989, in Hunt J., Battrick B. (eds.) Proc. 23rd ESLAB Symp. on two topics in X-ray astronomy, ESA SP-296. ESA Publications Division, Noordwijk, 499
Lochner J.C., Swank J.H., Szymkowiak A.E., 1991, ApJ 376, 295
McHardy I.M., 1989, in Hunt J., Battrick B. (eds.) Proc. 23rd ESLAB Symp. on two topics in X-ray astronomy, ESA SP-296. ESA Publications Division, Noordwijk, 1111
Miller G.S., 1995, ApJ 441, 770
Miyamoto S., Kitamoto S., Iga S., et al., 1992, ApJ 391, L21
Miyamoto S., Kitamoto S., Mitsuda K., Dotani T., 1988, Nat 336, 450
Mushotzky R.F., Done C., Pounds K.A., 1993, ARA&A 31, 717
Narayan R., 1996, ApJ 462, 136
Negoro H., Miyamoto S., Kitamoto S., 1994, ApJ 423, L127
Nolan P.L., Gruber D.E., Matteson J.L., et al., 1981, ApJ 246, 494
Nowak M.A., Dove J.B., Vaughan B.A., et al., 1998, in Scarsi L., Bradt H., Giommi P., Fiore F. (eds.) The Active X-ray Sky: Results from BeppoSAX and Rossi-XTE, Nuclear Physics B, Proc. Supp. Elsevier Science, in press
Nowak M.A., Vaughan B.A., 1996, MNRAS 280, 227
Oda M., Gorenstein P., Gursky H., et al., 1971, ApJ 166, L1
Parmar A.N., Lammers U., Angelini L., 1995, Legacy 6, 27
Payne D.G., 1980, ApJ 237, 951
Priedhorsky W., Garmire G.P., Rothschild R., et al., 1979, ApJ 233, 350
Robinson E.L., Nather R.E., 1979, ApJS 39, 461
Scargle J.D., 1981, ApJS 45, 1
Scargle J.D., 1982, ApJ 263, 835
Stella L., White N.E., Davelaar J., et al., 1985, ApJ 288, L45
Terrell N.J., 1972, ApJ 174, L35
Timmer J., 1995, Vorverarbeitung, Modellierung und Klassifikation von Zeitreihen. Harri Deutsch, Frankfurt, 1st edition
Unno W., Yoneyama T., Urata K., et al., 1990, PASJ 42, 269
van der Klis M., 1989, in Ögelman H., van den Heuvel E.P.J. (eds.) Timing Neutron Stars, NATO ASI C262. Kluwer Academic Publishers, Dordrecht, 27
van der Klis M., 1995, in Lewin W.H.G., van Paradijs J., van den Heuvel E.P.J. (eds.) X-ray Binaries. Cambridge Univ. Press, Cambridge, 252
Vaughan B.A., Nowak M.A., 1997, ApJ 474, L43
Vikhlinin A., Churazov E., Gilfanov M., et al., 1994, ApJ 424, 395
Voges W., Atmanspacher H., Scheingraber H., 1987, ApJ 320, 794
Wilms J., Dove J., Nowak M.A., Vaughan B., 1997, in Dermer C.D., Strickman M.S., Kurfess J.D. (eds.) Proc. 4th Compton Symposium, AIP Conf. Proc. 410. AIP, Woodbury, 849
Yule G.U., 1927, Phil. Trans. R. Soc. A 226, 304
Zhang W., Jahoda K., Swank J.H., et al., 1995, ApJ 449, 930